**Atmospheric
Chemistry
and Physics**

Modelling microphysical and meteorological controls on precipitation and cloud cellular structures in Southeast Pacific stratocumulus

H. Wang[1,2,*], **G. Feingold**[2], **R. Wood**[3], **and J. Kazil**[1,2]

[1]Cooperative Institute for Research in Environmental Sciences (CIRES), University of Colorado, Boulder, Colorado, USA
[2]NOAA Earth System Research Laboratory (ESRL), Boulder, Colorado, USA
[3]Department of Atmospheric Sciences, University of Washington, Seattle, Washington, USA
[*]now at: Pacific Northwest National Laboratory (PNNL), Richland, Washington, USA

Abstract. Microphysical and meteorological controls on the formation of open and closed cellular structures in the Southeast Pacific are explored using model simulations based on aircraft observations during the VAMOS Ocean-Cloud-Atmosphere-Land Study Regional Experiment (VOCALS-REx). The effectiveness of factors such as boundary-layer moisture and temperature perturbations, surface heat and moisture fluxes, large-scale vertical motion and solar heating in promoting drizzle and open cell formation for prescribed aerosol number concentrations is explored. For the case considered, drizzle and subsequent open cell formation over a broad region are more sensitive to the observed boundary-layer moisture and temperature perturbations ($+0.9\,\mathrm{g\,kg^{-1}}$; $-1\,\mathrm{K}$) than to a five-fold decrease in aerosol number concentration (150 vs. $30\,\mathrm{mg^{-1}}$). When embedding the perturbations in closed cells, local drizzle and pockets of open cell (POC) formation respond faster to the aerosol reduction than to the moisture increase, but the latter generates stronger and more persistent drizzle. A local negative perturbation in temperature drives a mesoscale circulation that prevents local drizzle formation but promotes it in a remote area where lower-level horizontal transport of moisture is blocked and converges to enhance liquid water path. This represents a potential mechanism for POC formation in the Southeast Pacific stratocumulus region whereby the circulation is triggered by strong precipitation in adjacent broad regions of open cells. A simulation that attempts to mimic the influence of a coastally induced upsidence wave results in an increase in cloud water but this alone is insufficient to initiate drizzle. An increase of surface sensible heat flux is also effective in triggering local drizzle and POC formation.

Both open and closed cells simulated with observed initial conditions exhibit distinct diurnal variations in cloud properties. A stratocumulus deck that breaks up due solely to solar heating can recover at night. Precipitation in the open-cell cases depletes the aerosol to the extent that cloud formation is significantly suppressed within one diurnal cycle. A replenishment rate of cloud condensation nuclei of order $1\,\mathrm{mg^{-1}\,h^{-1}}$ is sufficient to maintain clouds and prevent the boundary layer from collapsing the following day, suggesting that some local and/or remote aerosol sources is necessary for POCs to be able to last for days.

1 Introduction

The starkly different reflectance patterns associated with the frequent open and closed cellular structures in the Southeast Pacific (SEP) stratocumulus region as revealed by satellite imagery (e.g., Wood and Hartmann, 2006) are of great interest from the perspective of planetary albedo and climate change. Aerosol-cloud-precipitation interactions and associated dynamical feedbacks, large-scale forcing, meteorological conditions and other marine boundary layer processes are important components of the SEP climate system but are not well understood. How these components work together to control the formation and evolution of open and closed cellular structures is still an outstanding question. Observations from the Variability of the American Monsoon Systems (VAMOS) Ocean-Cloud-Atmosphere-Land Study Regional

Experiment (VOCALS-REx) and others support the hypothesis that drizzle is a necessary condition for the formation and maintenance of pockets of open cells (POCs) that are embedded within closed-cell stratocumulus (Comstock et al., 2005; Stevens et al., 2005b; Sharon et al., 2006; Wood et al., 2008, 2010). Recent large-eddy simulations and cloud-resolving modeling studies (e.g., Savic-Jovcic and Stevens 2008; Xue et al., 2008; Wang and Feingold, 2009a, b) have also demonstrated that drizzle, initiated by low aerosol concentrations in model simulations, can trigger the formation of open cellular structures. The process is accelerated by the steady depletion of the aerosol concentration by coalescence scavenging, that further increases drizzle until a super-clean state is reached (Sharon et al., 2006).

What exactly initiates precipitation and POCs in SEP stratocumulus in the first place is still unclear. Cloud drops have to attain sizes large enough to fall below cloud and evaporate during their fall, which depends on both cloud microphysics and dynamics. Factors that affect cloud microphysics, precipitation and boundary-layer dynamics include aerosol properties, boundary-layer relative humidity, surface heat and moisture fluxes, large-scale vertical motion and solar radiation. Previous observational studies (e.g., Stevens et al., 2005b; Sharon et al., 2006; Wood and Hartmann 2006) found no significant meteorological differences between the POC region and neighboring closed cells, suggesting that prior to the onset of precipitation POCs share the same large-scale and boundary-layer meteorological environments with neighboring closed cells. The possibility that drizzle and POCs are initiated by humid air above the inversion layer can be ruled out because the free-tropospheric air over both POC and closed-cell regions in the VOCALS-REx domain was extremely dry (e.g., Bretherton et al., 2010). Wood et al. (2008) also found that free-tropospheric moisture is not an important factor in POC formation over the SEP. The existing evidence supports low cloud condensation nuclei (CCN) concentrations as a trigger for drizzle formation in closed cells. There is substantial observational evidence that CCN and cloud drop number concentrations in POC regions are lower than in neighboring closed cells and that low drop concentrations in the stratocumulus decks of the SEP region favor POC formation (e.g., Petters et al., 2006; Wood et al., 2008); this, however, is not sufficient to identify whether the observed low CCN concentrations in POCs is the initial cause, or the consequence, of drizzle. It is difficult, if not impossible, to establish why CCN concentrations in POCs can suddenly become much lower than in the nearby closed cells prior to the onset of precipitation. All these unsolved puzzles motivate us to seek other possible answers from the factors that control cloud liquid water, which is the primary determinant of drizzle. Cooler and moister subcloud-layer air has been observed in regions that spawn POCs (e.g., Stevens et al., 2005b; Sharon et al., 2006, who referred to these features as "rifts"). Although this is at least partly a consequence of processes associated with drizzle in POCs (Stevens et al., 2005b;

Savic-Jovcic and Stevens, 2008; Wang and Feingold, 2009a, b), the possibility that POCs are initiated in moister and/or cooler air that is embedded within the closed-cell boundary layer could not be excluded.

Longwave radiative cooling near cloud top is very important for maintaining a solid stratocumulus deck. Substantial reduction of this cooling by solar radiation in the daytime may lead to thinning of clouds and even decoupling of the cloud layer from the sub-cloud layer (Nicholls, 1984). As a result, breakup of the solid deck is more likely to occur during the day. This has also been discussed as a process that might promote the transition of closed cells to open cells (Savic-Jovcic and Stevens, 2008), although one must distinguish between the open cellular structure and a stratocumulus deck that is simply more broken. A strong diurnal cycle of cloud fraction, liquid water path (LWP) and precipitation driven by local diabatic processes was observed over the SEP stratocumulus region during the East Pacific Investigation of Climate (EPIC) field experiment (Bretherton et al., 2004). Wood et al. (2008) found that most POCs visually identified on two-month satellite imagery over the SEP form during the early morning hours (0–6 h local time), indicating that solar radiation is not a necessary condition for POC formation. Using both ship and satellite measurements, they also show a noticeable diurnal variation of precipitation rate and cloud fraction when POCs were advected over the ship. This warrants further investigation of the diurnal cycle of cloud properties in both closed- and open-cell regions.

In this modeling study, potential factors such as boundary-layer relative humidity, surface heat and moisture fluxes, large-scale vertical motion (caused by different mechanisms) and solar heating are examined for their effectiveness in promoting drizzle and POC formation for prescribed aerosol concentrations. Simulations are mostly based on data sampled during the National Center for Atmospheric Research (NCAR) C-130 Research Flight 6 (hereafter, RF06) of VOCALS-REx.

2   Case description and model settings

RF06 (28 October 2008) was one of the VOCALS POC-drift missions (Wood et al., 2010) during which a mature POC embedded in an overcast stratocumulus deck was sampled at four levels (near-surface, near cumulus cloud-base, in-cloud, and the lower free-troposphere). Leg-mean measurements of potential temperature θ, water vapor mixing ratio q_v and horizontal winds are used to construct vertical profiles (Fig. 1) to initiate model simulations. The POC region, adjacent overcast region, and POC-overcast precipitating boundary are characterized separately. There are marked differences in observed θ and q_v in the boundary layer amongst the three regions. The inversion layer in the overcast and POC regions is located at about 1375 m (see Wood et al., 2010). In the overcast region the inversion is very sharp

and estimated to be ~50 m thick. In the POC region the inversion base height is more variable than in the overcast region. With the assumption that air below the inversion base is initially well-mixed, two sets of temperature and total water profiles are constructed from observations over the POC and nearby overcast regions, with values chosen to approximately match those in the surface layer of the overcast and POC regions. Boundary-layer air in the POC region is 1 K cooler and 0.9 g kg^{-1} wetter than in the overcast region (hereafter, wetter and drier soundings). The temperature and moisture jumps across the inversion in drier (wetter) sounding are 13 (13) K and 7.3 (8.0) g kg^{-1}, respectively. Profiles of wind components (u and v) are obtained from a fit to the leg-mean values but with an added reasonable wind-shear near the inversion. When winds are included in simulations, a Galilean transformation of -6 and 7 m s^{-1} is applied to u and v. The wetter and cooler sounding in the POC region results in a lower surface latent heat flux (observed latent heat fluxes, estimated using a bulk approach, are 122 in the POC and 148 W m^{-2} in the overcast) but greater sensible heat flux (15 vs. 3 W m^{-2}) than in the overcast region. Details of the surface heat flux measurements are provided in Wood et al. (2010). The daily mean, large-scale surface divergence in the domain (78–82 W, 15–21 S) is estimated from Quicksat surface winds to be 1.67×10^{-6} s^{-1}. If this surface divergence is held constant over the entire depth of the boundary layer, it results in a large-scale vertical velocity of -0.0025 m s^{-1} at 1.5 km, which is comparable to the -0.002 m s^{-1} obtained from the National Center for Environmental Prediction (NCEP) reanalysis. The surface friction velocity is set to 0.2 m s^{-1}.

The most up-to-date version of the Advanced Research Weather Research and Forecasting (ARW) model (v3.1) was used to perform high-resolution, cloud-resolving simulations. As in our previous studies (Wang and Feingold 2009a, b), a high-order monotonic advection scheme (Wang et al., 2009) and a double-moment bulk microphysical scheme (Feingold et al., 1998) are used. The simulated microphysical processes (activation, condensation/evaporation, stochastic collection and sedimentation) are also briefly described by Wang and Feingold (2009a). Lognormal basis functions are assumed to represent CCN, cloud and rain drop size distributions. A geometric standard deviation of 1.5, 1.2 and 1.2 is assumed, for each category, respectively. The cutoff diameter between the cloud and rain size distributions is 50 μm. For simplicity, particles are assumed to be composed of sea salt with a mean dry diameter of 0.2 μm, which is in broad agreement with the marine boundary layer aerosol and the observed accumulation-mode aerosol spectrum in RF06 which had a peak diameter of ~0.2 μm for particles in the range of 0.12–3.12 μm (Wood et al., 2010). Changes in the CCN are represented by changes in aerosol concentration alone; sensitivity to the aerosol size distribution and composition are not considered. These assumptions are unlikely to have significant influence on the results (Feingold, 2003). Longwave
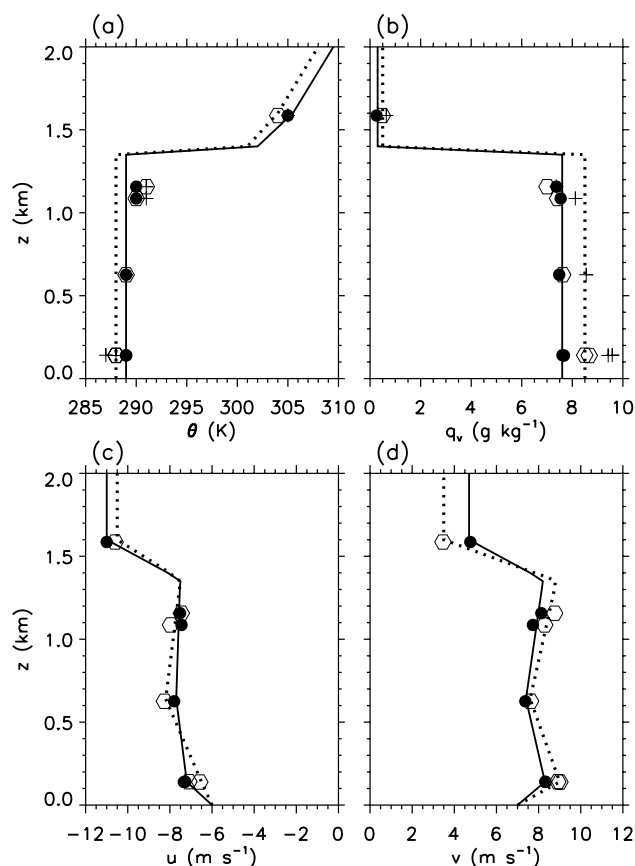

Fig. 1. Vertical profiles of **(a)** potential temperature θ, **(b)** water vapor mixing ratio q_v, and **(c, d)** horizontal winds u and v. Black circles, hexagons and plus signs represent RF06 leg-mean measurements for overcast regions, POCs and drizzling boundaries. Solid lines and dotted lines are profiles assumed for drier and wetter conditions for model simulations.

radiation is represented using the 16-spectral-band Rapid Radiative Transfer Model (RRTM; Mlawer et al., 1997), which utilizes the correlated-k method to calculate fluxes, and heating rates. For shortwave radiation, a scheme described by Dudhia (1989) is applied to account for downward integration of solar flux, clear-air scattering, water vapor absorption, and cloud albedo and absorption. Absorption and scattering by the aerosol is neglected.

Two sets of experiments are summarized in Table 1. In the first set, six experiments (D30, D150, D500, W30, W150 and W500) are performed to examine the diurnal cycle of cloud properties under different meteorological conditions for given initial CCN concentrations which are prescribed as 30, 150 and 500 mg^{-1} (mg^{-1} is roughly equivalent to cm^{-3}) to represent clean, moderately polluted and polluted marine conditions. "D" and "W" indicate the drier and wetter initial soundings, as shown in Fig. 1, along with the corresponding surface sensible and latent heat fluxes. In the second set, experiments PCCN, PQV, PTH, PQVT, PSFX,

Table 1. Summary of numerical experiments; the first set is for diurnal cycles and the second set is for sensitivity study; "drier" (boundary layer $q_v = 7.6$ g kg^{-1}; $\theta = 289$ K) and "wetter" ($q_v = 8.5$ g kg^{-1}; $\theta = 288$ K) soundings are depicted in Fig. 1; perturbations in the second set are applied to the center 30×30 km^2 of the domain in a spatially random fashion.

Experiment	q_v and θ profile	CCN conc. N_c (mg^{-1})	Solar radiation	Domain size (km^2)	Range of perturbation
D30	dry	30	yes	60×60	–
D150	dry	150	yes	60×60	–
D500	dry	500	yes	60×60	–
W30	wet	30	yes	60×60	–
W150	wet	150	yes	60×60	–
W500	wet	500	yes	60×60	–
CTRL	dry	150	no	90×90	none
PCCN	dry	150	no	90×90	$\Delta N_c \in (-120, 0)$ mg^{-1}
PQV	dry	150	no	90×90	$\Delta q_v \in (0, 0.9)$ g kg^{-1}
PTH	dry	150	no	90×90	$\Delta \theta \in (-1, 0)$ K
PQVT	dry	150	no	90×90	Δq_v and $\Delta \theta$
PSFX	dry	150	no	90×90	ΔSFX $\in (15, 30)$ W m^{-2}
PLFX	dry	150	no	90×90	ΔLFX $\in (150, 300)$ W m^{-2}
SLFX	dry	150	no	90×90	ΔSFX and ΔLFX
UPSW	dry	150	no	90×90	$\Delta w \in (0, 0.01)$ m s^{-1}

PLFX, SLFX and UPSW explore the effectiveness of a locally cleaner background (30–150 mg^{-1} vs. 150 mg^{-1}), a wetter (Δq_v= 0–0.9 g kg^{-1}) boundary layer, a cooler ($\Delta \theta$= -1–0 K) boundary layer, a wetter and cooler boundary layer, higher surface sensible heat fluxes (15–30 W m^{-2}), higher surface latent heat fluxes (150–300 W m^{-2}), higher sensible and latent heat fluxes and large-scale upsidence wave (0–0.01 m s^{-1}) in a predefined area at initiating drizzle within closed cells and their feedbacks on the surrounding closed cells. Except for the surface flux experiments, perturbations are applied through the depth of the boundary layer.

Perturbations in this second set of sensitivity experiments are applied to the inner 1/9 of the domain with a spatially random varying magnitude in the specified ranges (except for UPSW). In UPSW, a 15-km-wide upsidence wave (in the form of a positive-half sine wave; aligned uniformly in the y-direction; peak vertical velocity at 0.01 m s^{-1}) moves along the x-direction at 5 m s^{-1}. The control experiment (CTRL) has no aforementioned perturbations in the inner domain. All experiments in the second set are initiated with a CCN concentration of 150 mg^{-1}, the drier sounding without initial winds, and the corresponding surface heat fluxes, except for the aforementioned perturbations in each individual experiment.

The choice of the perturbation experiments and their meteorological context warrant some discussion. The magnitudes of the vapor and temperature perturbations are chosen to reflect the variability in observations associated with the RF06 flight between the precipitating open cell region and the overcast region. To be conservative, average perturbations of one-half of the observed differences in the soundings ($\Delta q_v = +0.9$ g kg^{-1}; $\Delta \theta = -1$ K) are applied in-

dividually and/or in unison. The surface CCN and surface flux perturbations are varied over reasonable ranges, reflecting natural variability, and in some cases are extended to probe parameter space. This approach is strongly rooted in the observations, as opposed to conforming to a theoretical framework in which simulations with a common denominator (such as lifted condensation level or buoyancy) are compared. For example, although the PQV and PTH experiments both increase relative humidity and therefore lower the lifted condensation level (by approximately 125 m and 50 m, respectively), no attempt has been made to require that these changes be the same. In the case of buoyancy, PQV and PTH even effect changes of opposite sign: +0.03% and -2% respectively. Forcing the perturbations to have the same effect on the lifted condensation level or buoyancy would be an interesting line of investigation, but would not be consistent with the observations.

The first set of simulations is performed in a 60×60 km^2 domain for 36 h, starting at local midnight, to cover one complete diurnal cycle after model spin up, while the second set is in a 90×90 km^2 domain for an 8-h nocturnal run. Cyclic boundary conditions are assumed in both x and y directions. The domain extends to 2 km in the vertical for all simulations with a damping layer in the upper 250 m. The horizontal (vertical) grid spacing is 300 (30) m, which has been demonstrated to be a reasonable compromise in these relatively large domain sizes (Wang and Feingold, 2009a). The effect of the relatively coarse horizontal grid is to reduce vertical mixing and generate more cumulus-like convection, potentially hastening the transition to open cells (see Wang and Feingold (2009a) for further discussion). The time step is 3 s.
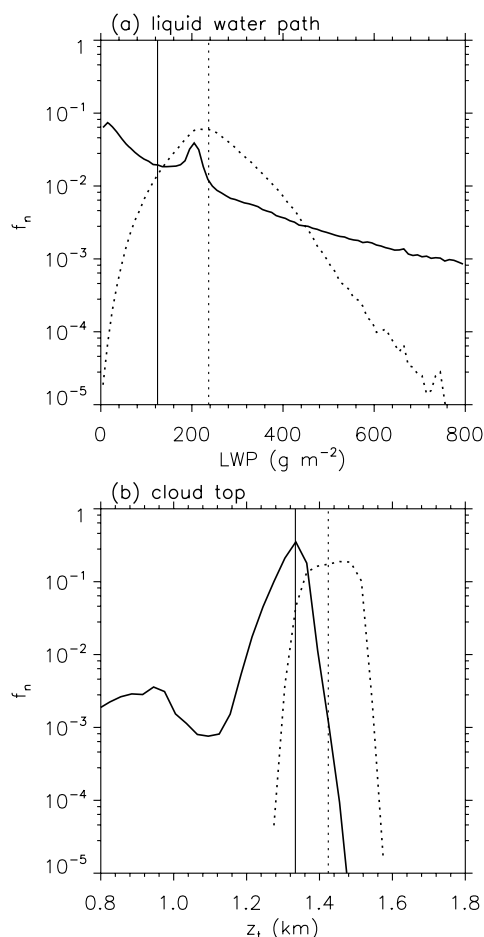
Fig. 2. Normalized probability distribution functions (PDFs) of **(a)** LWP and **(b)** cloud top height in the first 8 h from experiments D30 (solid lines) and D500 (dotted lines) with corresponding median values indicated by vertical lines. Cloud top in each model column is defined as the uppermost grid point that has cloud water mixing ratio $\geq 0.01\,\mathrm{g\,kg^{-1}}$.

3 Results

Before embarking on presentation of the control and sensitivity experiments, it is important to establish that the simulations provide a sufficiently high degree of realism to lend themselves to our experimental strategy. To this end we compare the statistics of a few key model fields such as liquid water path and cloud-top-height to observations. This should not be viewed as a rigorous intercomparison of modeled and observed fields, but rather as providing confidence that the control simulation represents the observed cloud fields sufficiently well that it can be considered an adequate framework within which to perform the sensitivity experiments.

Normalized probability distribution functions (PDFs) of simulated LWP and cloud top heights are shown in Fig. 2 for D30 (in which open cells form) and D500 (in which closed cells form). The PDFs represent averages over the first eight

hours of simulation and therefore represent nocturnal conditions. The PDFs capture the characteristic differences between open and closed cell simulations; open-cell PDFs are much broader and contain a tail of high LWP associated with the vigorous open-cell walls, as well as a large number of small LWP events associated with decaying open cell walls that have evolved into thin cloud in the cell centers (Wood and Hartmann, 2006; Wang and Feingold, 2009a). In contrast, the closed-cell LWP PDF has a narrower distribution with a distinct maximum. Comparison with the observed values of LWP from the RF06 measurements (Wood et al., 2010) shows that the model captures the characteristics of the PDFs remarkably well; median values of LWP for the open cells are $125\,\mathrm{g\,m^{-2}}$ (model) and $125\,\mathrm{g\,m^{-2}}$ (observations). For the closed cells the model yields a median value of $237\,\mathrm{g\,m^{-2}}$ and the observations $215\,\mathrm{g\,m^{-2}}$.

PDFs of cloud-top-height show a higher cloud top for the closed cell than for the open cell simulation. Although initiated with the same sounding, and therefore the same cloud-top height, closed-cell clouds in D500 grow higher than open-cell clouds (D30) because of persistently stronger radiative cooling over the closed-cell deck and the suppression of entrainment due to precipitation in D30 (e.g., Stevens et al., 1998). The long tail and a second peak in the cloud-top distribution in D30 are contributed by small penetrating cumulus clouds and decaying open-cell walls. However, the observed bimodality (i.e., higher wall clouds with peaks at ~1450 m, and lower decaying clouds with peaks at ~ 1350 m; Wood et al., 2010) of open-cell cloud tops is not well reflected in Fig. 2, and the median simulated closed cell tops are about 70-m higher than the observed ones. The spatial and temporal sampling over the entire domain for a period of a few hours during which time clouds are progressively evolving obscures the variation of cloud tops between open-cell walls and decaying cells. Similarly temporal averaging of a progressively increasing cloud-top over 8 h also causes a high bias in simulated cloud-top-height compared to the initial observed values. These differences are noted but are not expected to have significant bearing on the results to be presented below.

3.1 Diurnal cycle of open and closed cells

Results from the first set of simulations with spatially homogeneous CCN concentrations, initial sounding profiles, surface fluxes, and large-scale subsidence, are presented to illustrate the diurnal cycle of stratocumulus clouds induced by solar heating. Different aerosol scenarios and meteorological conditions are prescribed to initiate either closed cells or drizzle and the formation of open cells. Figure 3 shows the diurnal variations of cloud properties in the six experiments with different combinations of aerosol and meteorological conditions. Cloud fraction, LWP and rain rate have a strong diurnal cycle with a late-afternoon minimum, which is similar to EPIC observations (e.g., Bretherton et al., 2004)
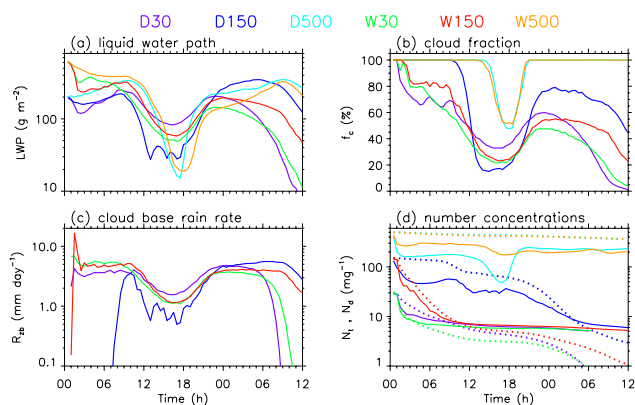
Fig. 3. Time evolution of **(a)** domain-average LWP; **(b)** cloud fraction; **(c)** domain-average cloud-base rain rate R_{zb}; and **(d)** cloud-average drop number concentration N_d (solid) and boundary-layer total particle number concentration N_t (dotted) for the six experiments as indicated in the legend. Cloudy columns are defined by optical depth >2 for the calculation of cloud fraction; a threshold of $N_d = 5\,\mathrm{mg}^{-1}$ is applied when calculating cloud-average N_d. Cloud base in each model column is defined as the lowest grid point that has cloud water mixing ratio $\geq 0.01\,\mathrm{g\,kg}^{-1}$.

and other LES results (e.g., Caldwell and Bretherton, 2009). Drizzle develops quickly in D30, W30 and W150. Although the initial drop number concentration N_d is enhanced by a factor of 5 in W150, compared to D30, the larger LWP (600 vs. 200 g m^{-2}) generated by the wetter sounding overcomes the initial N_d barrier, initiates drizzle, reduces N_d significantly, and eventually develops even stronger drizzle. The stronger dependence of cloud-base rain rate R_{zb} on LWP than on N_d is consistent with modeling results in a shallower marine boundary layer (e.g., Wang and Feingold, 2009a) and observational studies (Pawlowska and Brenguier, 2003; van-Zanten et al., 2005; Sorooshian et al., 2009; Kubar et al., 2009; Wood et al., 2009). This reinforces the notion that drizzle is more sensitive to the meteorological conditions that control LWP than to the aerosol perturbation.

Open cellular structures develop in the three cases that have early drizzle formation. During the daytime, solar heating breaks up open-cell walls and cloud fractions are further reduced (Fig. 3a, b). We note, however, that solar heating is likely overestimated in the simulations and consequently, the daytime reduction of cloud water and precipitation is probably also overestimated. Clouds initially form a closed-cell structure in D150 but open cells start to form in association with the reduction in N_d and initiation of precipitation. However, solar heating hinders the development of solid open-cell walls, causing a rapid reduction in cloud fraction (from overcast to 15% in 4 h) and in LWP. This has been demonstrated in a sensitivity test that excludes solar heating in D150 (results not shown here).
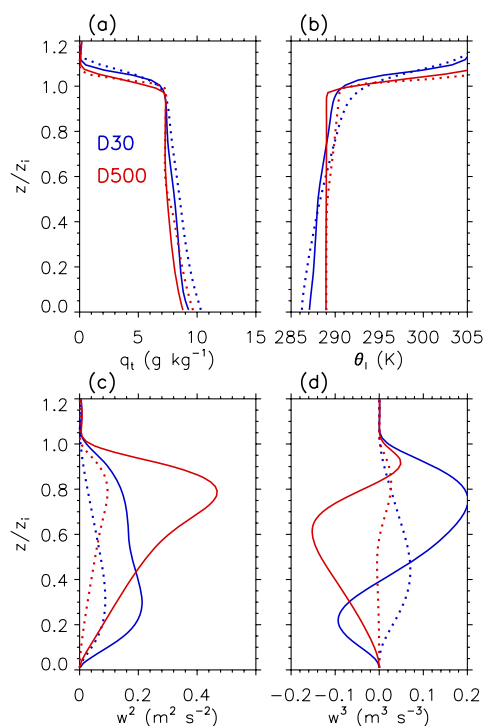

Fig. 4. Vertical profiles of **(a)** total water mixing ratio q_t, **(b)** liquid water potential temperature θ_l, **(c)** variance of vertical velocity $\overline{w'^2}$, and **(d)** third moment of vertical velocity $\overline{w'^3}$. Profiles are domain-averages at night between $t = 3$ and 9 h (solid) and in the day between $t = 9$ and 15 h (dotted). Note that vertical axis is normalized by the corresponding mean inversion base height, which is larger in D500 than in D30.

In the two polluted cases D500 and W500, insignificant amounts of in-cloud drizzle ($R_{zb} < 0.1\,\mathrm{mm\,day}^{-1}$) are formed. Although cloud fraction decreases to 50% and LWP to less than 20 g m^{-2}, a closed cellular structure recovers during the subsequent night; however, closed cells do not reform in other cases where precipitation has developed. This suggests that solar heating temporarily breaks up closed cells but precipitation is necessary for the formation of open cells. We thus distinguish between broken cloud resulting from daytime heating and organized open cellular structures.

The reduction of turbulent mixing and cloud water in the daytime is caused by solar heating due to the short-wave absorption by cloud water and water vapor, which has long been suggested to cause decoupling in the stratocumulus-topped marine boundary layer (e.g., Nicholls, 1984). Vertical profiles shown in Fig. 4 demonstrate the day/night contrast in turbulence and thermodynamics for D30 and D500. Overall, D500 has a much drier cloud layer (i.e., the upper boundary layer where clouds are present) than D30 because of more entrainment. The cloud layer is significantly warmed in the day and the boundary layer becomes more stable. Moisture supply from the surface is cut off. The sub-cloud humid layer is

decoupled from the overlying clouds, which become thinner and even dissipate. For the precipitating open-cell case, sedimentation and evaporation of rain drops cool and moisten the sub-cloud layer, stabilizing the boundary layer as well. Daytime warming of the cloud layer in D500 is mainly induced by cloud absorption of solar radiation. Even though cloud cover in D30 is relatively small, water vapor absorption can play a similar role to cloud absorption in stabilizing the boundary layer and reducing turbulence (Wang and McFarquhar 2008). This, together with the effect of drizzle, explains why the cloud layer in D30 is even warmer and less turbulent than in D500.

Turbulent mixing in the day is weaker, as indicated by the variance of vertical velocity $\overline{w'^2}$. The strong day-night contrast is consistent with simulations by Caldwell and Bretherton (2009). It is noteworthy that $\overline{w'^2}$ tends to be underestimated in the simulations due to the coarse horizontal grid size (Wang et al., 2009), particularly, during the day when solar heating is likely overestimated by the radiation model. Nevertheless, comparison between early morning aircraft measurements of $\overline{w'^2}$ and nighttime model-derived values show surprisingly good agreement; peak nighttime modeled values of $\overline{w'^2}$ are approximately 0.5 m² s⁻² and 0.2 m² s⁻² for closed and open cell conditions (Fig. 4), as compared to rough estimates of 0.6 m² s⁻² and 0.3 m² s⁻² for early morning observations (Wood et al., 2010). As discussed by Stevens et al. (2005a), predominantly negative $\overline{w'^3}$ in D500 indicates strong downdrafts driven by radiative cooling which is largely reduced in the day. Positive $\overline{w'^3}$ in D30 is indicative of cumuliform convection. The sub-cloud negative $\overline{w'^3}$ in D30 at night is contributed by downdrafts associated with precipitation. Stabilization and decoupling of the cloud layer in the day causes the flat $\overline{w'^3}$ profile in both cases.

Fewer CCN are activated in the much less turbulent boundary layer during the day, as shown in Fig. 3 (D500 and W500 cases). This diurnal cycle in N_d does not appear in the precipitating cases, where CCN have been highly depleted. Without a replenishing CCN source, clouds in the boundary layer collapse completely by the second day. Sensitivity tests with different CCN source strengths show that under these super-clean conditions even a very weak CCN source can help maintain the clouds. This is discussed in Sect. 4.1.

3.2 Impact of CCN and meteorological perturbations on POC formation

Previous modeling studies (e.g., Savic-Jovcic and Stevens, 2008; Xue et al., 2008; Wang and Feingold, 2009a, b) have demonstrated that lower CCN concentrations can initiate drizzle and trigger the formation of open cellular structures in a certain meteorological environment. Results from the sim-
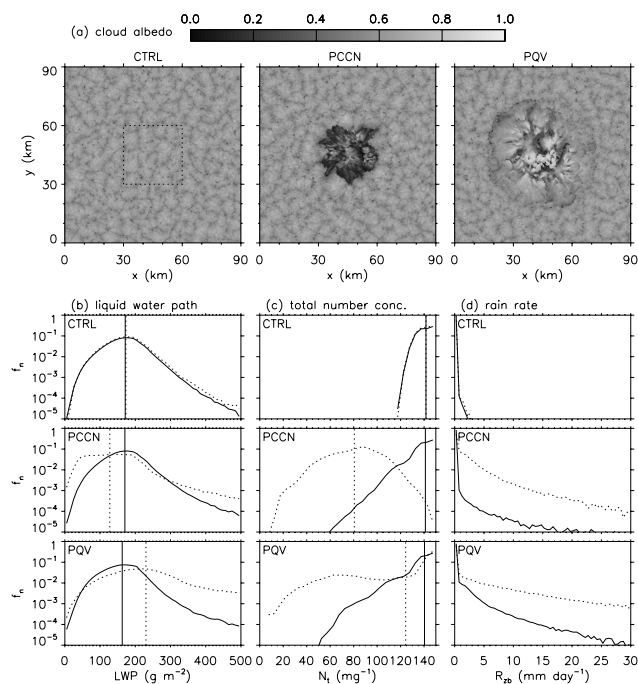

Fig. 5. Snapshots of **(a)** cloud albedo fields at $t = 6$ h and normalized PDFs of **(b)** liquid water path, **(c)** column-average total particle number concentration, and **(d)** cloud-base rain rate over 8 h for experiments CTRL, PCCN and PQV. The center-square outlined by dotted lines in the upper-left panel is the area in which specific perturbations are applied; distributions of quantities sampled inside the square are represented by dotted lines and outside by solid lines; the corresponding vertical lines indicate median values.

ulations with different soundings in the present study suggest that varying meteorological conditions can also change cloud cellular structures for prescribed CCN concentrations. Sensitivity experiments PCCN, PQV, PTH and PQVT are performed to examine the extent to which reasonable perturbations in CCN concentration and boundary-layer moisture and/or temperature in an embedded area are capable of opening the closed cells. Since individual snapshots are presented we do not explicitly show the temporal evolution of the open-cellular structures, nor do we dwell on the morphological features of open and closed cellular structures that have been described elsewhere. As will be seen below, some of the perturbations appear to have similar features to actinoform clouds (Garay et al., 2004). As will be shown in the following discussion, the prescribed CCN number concentration and moisture perturbations effectively initiate local POC formation in the otherwise closed cells (Fig. 5a); however, the combination of perturbations in moisture/temperature and temperature alone initiate drizzle and POC formation in *neighboring* closed cells (Fig. 6a) rather than in the locally perturbed area.
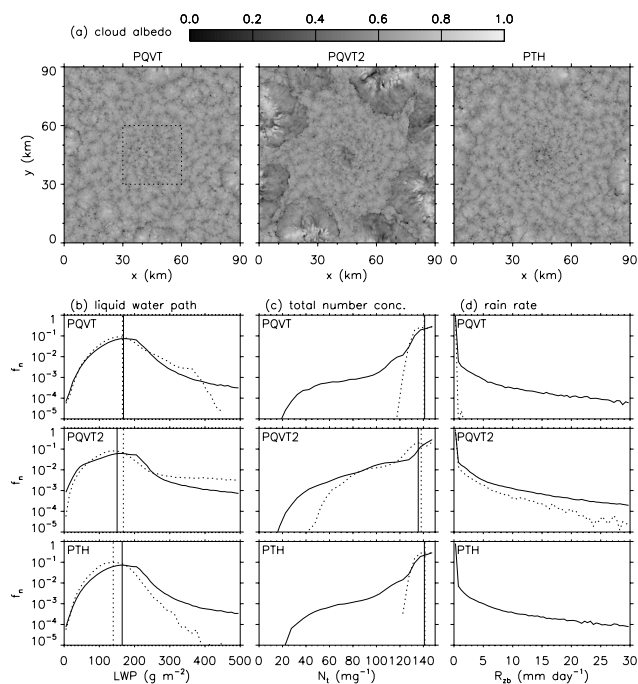
Fig. 6. Same as Fig. 5 but for experiments PQVT, PQVT2 and PTH.

Snapshots of cloud albedo and normalized PDFs of LWP, total number concentration (aerosol plus drops; N_t) and cloud-base rain rate for sensitivity experiments PCCN and PQV together with the control experiment CTRL are plotted in Fig. 5. In CTRL, although the LWP distribution is broadened from an initial homogeneous value of $200\,g\,m^{-2}$, the N_t distribution remains narrow and almost no rain develops in 8 hours. The CCN number concentration perturbations in PCCN effectively initiate drizzle, which further reduces N_t and progressively broadens the LWP distribution, causing the formation of open cells in the perturbed area. Drizzle tends to broaden the LWP distribution to both larger and smaller values and to flatten it at intermediate values (see also Fig. 2). The influence of CCN perturbations also propagates to the neighboring closed cells as seen in the changes in distributions compared to CTRL.

An addition of moisture to the inner domain of PQV significantly enhances local LWP (Fig. 5b), generating drizzle that exceeds that in PCCN. The N_t distribution in PQV is broadened commensurately and extends to lower values. Drizzle is delayed in PQV compared to PCCN; e.g., PQV has a mean cloud-base rain rate of less than $0.02\,mm\,day^{-1}$ at $t = 4\,h$ (not shown) simply because the much smaller drops need time to take advantage of the additional water vapor and are much less efficient at collision-coalescence growth, suggesting that the effect of the moisture perturbation on a polluted environment is initially buffered by the system (Stevens and Feingold, 2009). Prior to drizzle formation, cloud drop size is equally determined by drop number concentration and liquid water content. A five-fold decrease in CCN number

concentration in PCCN can increase drop size much more efficiently than a 12% increase in water vapor in PQV (with its associated two-fold increase in LWP). Only if LWP is already high enough (i.e., for a given N_d, drops reach large enough sizes to fall below cloud), does rain rate become more sensitive to the relative increase of LWP than to the decrease in CCN number concentration.

The additional water vapor in PQV enables a locally sustained drizzle event, with the influence propagating to the neighboring closed cells. Drizzle and broken clouds manifesting open-cellular structure cover almost the entire domain by $t = 8\,h$ (not shown). In contrast, with the cessation of drizzle due to reduction in LWP by drizzle in PCCN, and no balancing source of water vapor, the POCs shrink notably.

The results of PQVT and PTH are plotted in Fig. 6 in the same way as in Fig. 5. Interestingly, clouds in the perturbed domain maintain a closed cellular structure throughout the simulation, as seen in Fig. 6 at $t = 6\,h$. Compared to the PQV case, PQVT has an even higher initial relative humidity in the perturbed boundary layer but no drizzle forms. LWP in the perturbed domain of PQVT is indeed enhanced significantly in the first few hours (e.g., a second peak at about $370\,g\,m^{-2}$ in Fig. 6b), however, it is still not high enough to trigger widespread drizzle under the moderately polluted conditions. In contrast, significant drizzle appears in the unperturbed part of the domain. In order to explore this further, an additional sensitivity experiment PQVT2 is conducted, in which the magnitude of moisture and temperature perturbations is doubled (i.e., mean $\Delta\theta = -1\,K$; mean $\Delta q_v = 0.9\,g\,kg^{-1}$). As expected, LWP (Fig. 6b) and drizzle (Fig. 6d) is strongly enhanced in the perturbed domain. The unperturbed domain also experiences significantly higher drizzle rates. Does this mean that the initial perturbations in PQVT are not strong enough? The answer is *no* because the moisture perturbation alone in PQV *is* strong enough to initiate drizzle and POCs. Moreover, POCs formed in the perturbed domain of PQVT2 disappear soon after their formation (See Fig. 6a). All these beg for other explanations.

As mentioned before, the impact of additional moisture on drizzle is buffered by other interactions in the system. What causes LWP to cease growing during the buffering time in both PQVT and PQVT2 but not in PQV? Analysis shows that the colder temperature in the inner perturbed domain in PQVT, PQVT2 and PTH triggers convergence of air from the surroundings, generating a pressure gradient in the boundary regions. The pressure gradient force drives a local circulation with a divergent (convergent) flow in the lower (upper) boundary layer. The circulation in PQVT is illustrated in Fig. 7 (left panels). This circulation transports the added water vapor (i.e., moisture perturbations) in the lower boundary layer and surface moisture fluxes out of the inner domain (see Fig. 7; contours in right panels). Initially (e.g., at $t = 1\,h$), clouds are thicker in the inner domain where water vapor perturbations are still high (and positive); however, the cutoff of moisture supply to the cloud layer prevents the
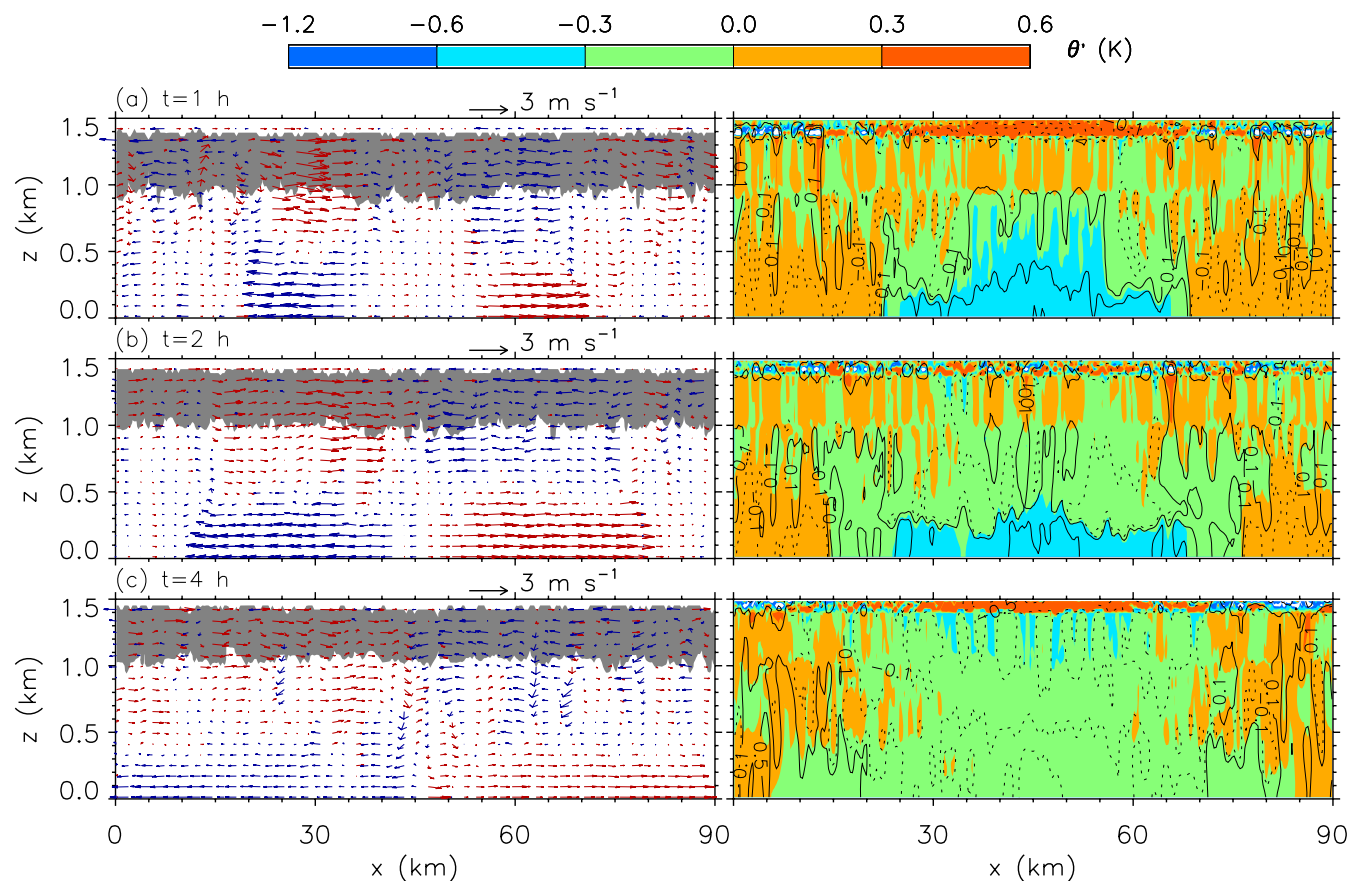
Fig. 7. The x-z cross-sections (at y = 45 km) from experiment PQVT at **(a)**–**(c)** t = 1, 2 and 4 h. Left: Gray shaded areas denote clouds (cloud water mixing ratio > 0.01 g kg^{-1}); arrows represent wind perturbations ($u - w$) with red for westerly ($u > 0$) and blue for easterly ($u < 0$) to demonstrate the outflow at the lower-level and return flow at the upper-level associated with the negative temperature perturbation in the middle of the domain (originally between $x = 30$ and 60 km). Right: Shaded colors indicate temperature perturbations, and contours, water vapor mixing ratio perturbations (positive by solid lines and negative by dotted lines); perturbations are relative to the horizontal slab average at each level.

further increase of LWP in the inner domain of PQVT. At the same time, the heterogeneous temperature perturbations in the inner domain (PQVT and PQVT2) result in circulations which act to mix air in different columns, smooth out the initial temperature and moisture perturbations, and avoid producing locally high LWPs that favor drizzle formation. The organized circulation expands to the entire domain by $t = 4$ h, and clouds become thinner in the perturbed area as water vapor is transported away. As the temperature gradient becomes weaker, the circulation weakens, in the absence of the additional moisture as in PQVT, LWP in the inner domain of PTH is strongly reduced (Fig. 6b). Compared to the CTRL case, the median LWP is over 25 g m^{-2} smaller and the distribution is narrower.

In both PQVT and PTH, the inner-domain N_t distribution is not affected at all by the perturbations because of a lack of drizzle, and looks much as it does in CTRL. However, moisture transported to the outer domain increases LWP there, and cloud-base rain rate is comparable to that of the per-

turbed domain in PCCN. Consequently, N_t is significantly reduced in the precipitating area (evidenced by the long tail in the frequency distribution), representing a positive feedback mechanism that accelerates the formation of open cells in an initially unperturbed area. The generation of mesoscale circulations associated with perturbations could have a potentially profound remote impact, and may represent a possible mechanism for initiating drizzle and POC formation in closed cells (see Sect. 4.2).

3.3 Impact of surface fluxes on POC formation

The impact of higher surface latent heat flux, sensible heat flux and the combination of both on POC formation is examined in PLFX, PSFX and SLFX, respectively. Larger surface fluxes exerted on the inner domain enhance temperature and/or moisture in the boundary layer. Figure 8 shows the results from these three experiments, plotted in the same way as for other sensitivity experiments (e.g., Figs. 5 and 6).
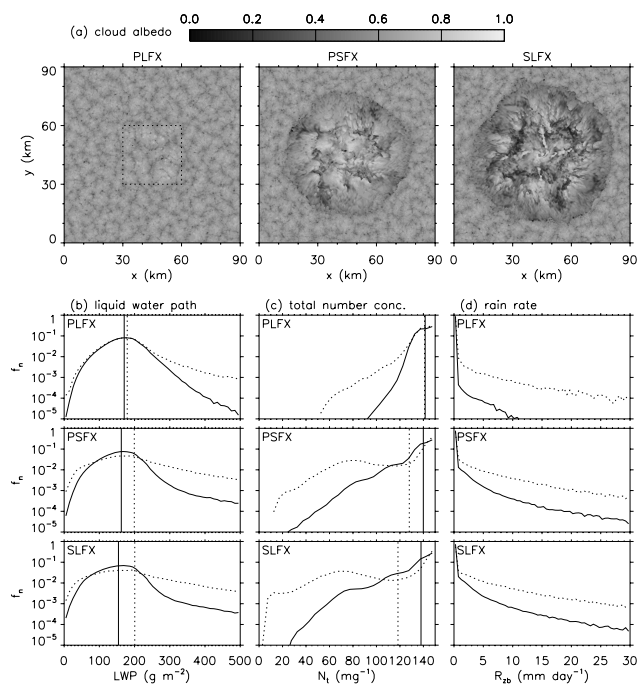
Fig. 8. Same as Fig. 5 but for experiments PLFX, PSFX and SLFX.

Overall, drizzle is eventually initiated in the inner domain of all three cases with the strongest in SLFX and the weakest in PLFX. There are two reasons for the stronger effect of surface sensible heat fluxes. First, accumulated moisture near the surface is effectively transported to the cloud layer by enhanced buoyancy of thermals due to stronger surface sensible heating. Second, a temperature gradient induced by stronger surface heating in the inner domain generates a circulation with convergent flow in the lower boundary layer that pumps moisture from the adjacent surface layer. This circulation is developed via the same thermal-gradient mechanism as described for PTH, but is opposite in direction; convergent (divergent) flow in the lower (upper) boundary layer. In PLFX, although the moisture supply from the surface is stronger than in PSFX, it is not effectively transported to the cloud layer to increase LWP. Therefore, drizzle in PLFX is initiated later, and the rain rate is the smallest of all. As in other precipitating cases, once drizzle is initiated in the inner domain, LWP and N_t distributions are broadened, resulting in stronger precipitation and the formation of POCs. The impact also propagates to the outer domain.

A possible concern is that the perturbation in surface sensible heat fluxes (15–30 W m^{-2}) is too strong, compared to the observed sensible heat flux of 3 W m^{-2} in the closed-cell region. To address this, another sensitivity test with weaker perturbations (10–20 W m^{-2}; mean value 15 W m^{-2}, equal to the one observed in the POC region) is performed. Results show no significant difference from the PSFX case, suggesting that it is the contrast in sensible heat fluxes between inner and outer domain that triggers drizzle and POC
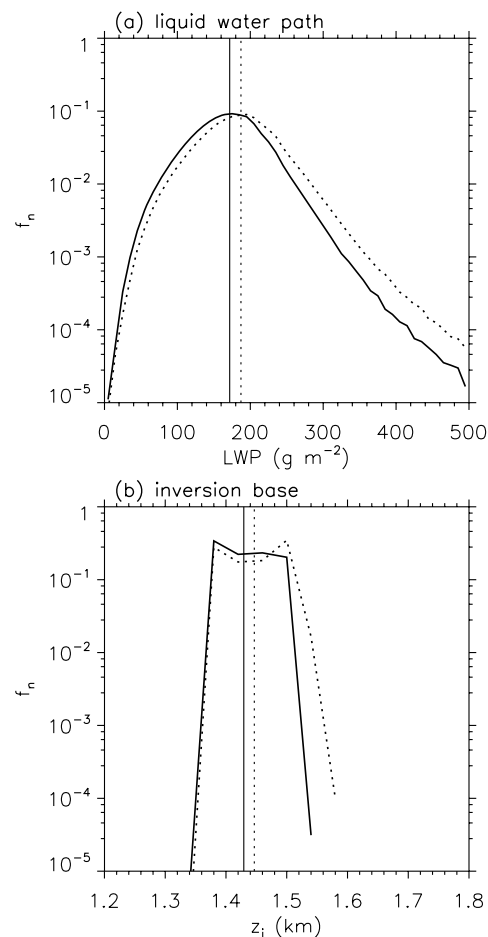

Fig. 9. Normalized frequency distributions of **(a)** liquid water path, **(b)** inversion base height over 8 h for experiments CTRL (solid lines) and UPSW (dotted lines) with the0 corresponding vertical lines indicating median values.

formation in the inner domain. The perturbation of surface latent heat fluxes (150–300 W m^{-2}) is likely too strong for the VOCALS-REx region and therefore the sensitivity test (PLFX) is a relatively extreme test of whether this enhancement could be an efficient way to initiate drizzle in closed cells. However, total heat fluxes associated with the broad open cells can range from 145 to 1200 W m^{-2} with the most frequent values being below 400 W m^{-2} (Atkinson and Zhang 1996), and so this test may still be broadly relevant.

3.4 Impact of large-scale vertical motion on POC formation

Large-scale vertical motion in the subtropical SEP region is generally dominated by subsidence associated with the descending branch of Hadley circulation. Garreaud and Muñoz (2004) and Rahn and Garreaud (2010) found that an "upsidence wave" produced by low-level convergent flow propagates from the coast of southern Peru to the SEP region. The

upsidence wave was also shown by their models to deepen the marine boundary layer, resulting in entrainment of more warm and dry air from the free-troposphere, and dissipation of clouds. It has been speculated that the upsidence wave may be an important factor in promoting the POC formation in the SEP region (René Garreaud, personal communication 2009). Our model domain is too small to simulate the upsidence wave; however, it is still of interest to evaluate whether the large-scale ascending motion associated with upsidence waves is sufficient to thicken the closed cells and initiate drizzle. In experiment UPSW, the closed cells in the model domain are exposed to the upsidence wave for a longer time than they should be, because the wave moves through the closed-cell domain at $18 \, \mathrm{km \, h^{-1}}$ instead of the $100 \, \mathrm{km \, h^{-1}}$ found by Garreaud and Muñoz (2004); this gives an upper bound on the LWP that closed cells in the "real" upsidence wave could achieve.

In experiment UPSW, the effects of the upsidence wave are simulated as a 15-km wide upward moving wave (in the form of positive-half sine wave with an amplitude of $0.01 \, \mathrm{m \, s^{-1}}$). Simulation results show that the assumed upsidence wave is not strong enough to have a significant impact on LWP and cloud cellular structures. Figure 9 shows the probability distribution function of LWP and boundary-layer depth (z_i) in UPSW in comparison to the control experiment CTRL. The median value of LWP is enhanced by $15 \, \mathrm{g \, m^{-2}}$. Although the maximum LWPs are increased by up to $150 \, \mathrm{g \, m^{-2}}$, they are too spatially sporadic to have a broad impact on the cloud structures in the moderately polluted environment. The boundary-layer depth, as indicated by the inversion base height in Fig. 9b, increases in the upsidence waves, which is consistent with simulations by Garreaud and Muñoz (2004). The median value is increased by $20 \, \mathrm{m}$.

The results suggest that the "upsidence wave" as observed by Garreaud and Muñoz (2004) and Rahn and Garreaud (2010) is unlikely to be the trigger of drizzle and POCs in closed cells, but this doesn't mean that an increase in local vertical velocity has no impact on the POC formation. As indicated in some of the other sensitivity experiments (e.g., PQVT, PQVT2), thickening of clouds and initiation of drizzle in neighboring unperturbed closed cells occurs through enhancement of vertical velocities; however, the magnitude (on the order of $1 \, \mathrm{m \, s^{-1}}$) is much larger than the prescribed large-scale upsidence in UPSW. The role of these relatively small-scale upsidence waves in promoting non-local drizzle and breakup of closed cells is discussed in the next section.

4 Discussion

4.1 Cloud formation suppressed in super-clean environment

As seen in the results of the strongly precipitating diurnal-cycle cases (D30, W30 and W150), without a replenishing source, CCN are depleted by precipitation scavenging and clouds in the boundary layer collapse completely by the second day because the super-clean environment cannot sustain clouds (Fig. 3). Sensitivity experiments (SA1, SP1, SA2 and SP2) are performed to test this hypothesis. They have the same settings as in D30 except for CCN source strength and/or starting time. The specific sources of CCN such as local nucleation, surface emission, and transport/advection from neighboring polluted regime or the free-troposphere, are not explicitly modeled in these simulations. Instead, a uniform source strength is assumed for the entire boundary layer. The source strengths of the first set (SA1 and SP1) and the second set (SA2 and SP2) are $3.6 \, \mathrm{mg^{-1} \, h^{-1}}$ and $0.72 \, \mathrm{mg^{-1} \, h^{-1}}$, respectively. These values bound the source strength of approximately $1.6 \, \mathrm{mg^{-1} \, h^{-1}}$ (Aitken + accumulation + coarse modes) derived from a parameterization of sea-salt production (Clarke et al., 2006) for this case. "A" and "P" indicate the source starting times of 6 a.m. and 6 p.m. (local time) on the first day, respectively. Figure 10 shows the time evolution of LWP, cloud fraction, R_{zb} and N_t in the four sensitivity experiment along with their control experiment D30. With the stronger source strength, total particle number concentration N_t is maintained at about the same magnitude as on the first morning, indicating that this source strength offsets approximately the loss of particles through precipitation scavenging. The local maximum at about 6 p.m. is due to the minimum rain rate and precipitation scavenging in the daytime. With the sustained N_t, LWP and R_{zb} become even larger on the second day because precipitation on the first day has created a boundary layer more conducive to cloud and rain formation. Although the boundary layer is still quite clean in these cases, even a weak source strength (i.e., $0.72 \, \mathrm{mg^{-1} \, h^{-1}}$) and prevents the boundary layer from collapsing during the course of the following day, suggesting that clouds in the clean environment in D30 are indeed suppressed and some local and/or remote CCN sources are necessary for open cells to be able to last for days. These super-clean conditions represent a situation of CCN-limited cloudiness.

4.2 Remote control of POC formation

In the previous section, it was shown that in some sensitivity experiments (i.e., PTH, PQVT, PQVT2) drizzle and POC formation occurred in the initially unperturbed closed cells instead of the area that experienced the perturbations directly. We refer to this as "remote control" of POC formation, which is realized by the perturbation promoting a mesoscale
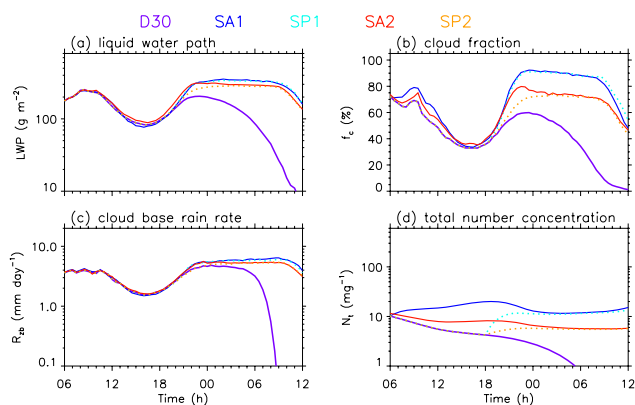
Fig. 10. As in Fig. 3 but for experiment D30 and four other sensitivity experiments with different CCN source strengths and start times. Note that the time axis is different from Fig. 3. The source strengths of the first set (SA1 and SP1) and the second set (SA2 and SP2) are $3.6\,\mathrm{mg}^{-1}\,\mathrm{h}^{-1}$ and $0.72\,\mathrm{mg}^{-1}\,\mathrm{h}^{-1}$. "A" and "P" indicate the source starting time of 6 a.m. and 6 p.m. (local time), respectively. Dotted linestyles are used to help distinguish between overlapping lines.

circulation that channels moisture from the near-surface layer to remote clouds. This circulation has a low-level horizontal branch which is rooted in the initially perturbed region, and a propagating ascending branch produced by the low-level convergent flow. It can be driven by the temperature gradient as seen in the present study or by the strong sub-cloud precipitation as simulated by Wang and Feingold (2009b). Once drizzle is initiated, positive feedbacks through enhancement of LWP and reduction in CCN accelerate the formation of open cells in the remote area.

We hypothesize that remote control of this kind may be a potential mechanism via which drizzle and POC formation can be initiated in closed cells. POCs or cloud rifts often appear in satellite images (e.g., GOES-10 imagery for October 19-28, 2008, in SEP, available at http://catalog.eol.ucar.edu/vocals/) in the form of arc shapes, not far from a broad region of open cells, with the concave side of the arc facing towards the open cells. This suggests that POCs may potentially be associated with ripple waves originating from the broad region of open cells.

To illustrate how the aforementioned circulation triggers POC formation in closed cells, another sensitivity experiment CTRL-QVT2, which has the same strength of initial perturbations in q_v and θ as in PQVT2, but otherwise the same settings as in CTRL, is performed in a $145 \times 60\,\mathrm{km}^2$ domain. The perturbations are applied to a strip aligned along the y-direction that covers the middle 15 km in the x-direction. This is to mimic a small portion of an arc-shaped wave in the marine boundary layer. Figure 11 shows the snapshots of vertical velocity w, water vapor mixing ratio q_v, rain rate and cloud albedo at three different times. The circulation bounded by the strong updrafts expands to both sides of the x-direction at about $25\,\mathrm{km}\,\mathrm{h}^{-1}$.

Water vapor is transported away from the source region in the lower-level horizontal branches. Clouds are thickened in the updrafts but still not enough to initiate drizzle in the first few hours. Only after the two propagating horizontal branches meet due to the cyclic boundary condition and force an even stronger convergence of water vapor, are clouds thick enough to start drizzling and form open cells. This suggests that if a single organized ascending branch of such a circulation is not strong enough to initiate drizzle, the convergence of two or more such circulations could accomplish the task.

Further simulation at larger scales than those simulated here would be required to strengthen the hypothesis of "remote-controlled" generation of POCs.

4.3 Marked differences in meteorological conditions: cause or effect of POCs?

Marked differences in q_v and θ between the open-cell region and overcast region were observed during RF06 (e.g., Fig. 1). Is there a causal relationship between these differences and POCs? If so, are the differences a result of, or perhaps the reason for, POC formation? The simulation results above have shown that POCs can form under both the "drier" and "wetter" conditions that were observed in overcast and open-cell regions, respectively, but the wetter conditions are more conducive to POC formation. However, it is unlikely that the POC region was locally significantly wetter and cooler than the neighboring closed cells prior to POC formation. Although water vapor can be transported to the POC region, the lower boundary layer in neighboring closed cells along the path can too be moistened due to transport. Model simulations initiated with the same initial q_v and θ profiles also give distinct evolved profiles for open-cell and closed-cell cases. Figure 12 shows q_v and θ profiles from experiments D30 and D500 where the same "drier" sounding (solid lines in Fig. 1) is used. Observations are included in the same plots for comparison. During the model spin-up time (first two hours), q_v and θ profiles for both D30 and D500 still follow the observed initial dry/warm conditions quite well. Over the next 6 h, q_v in the lower boundary layer in D500 is enhanced due to surface moisture fluxes but reduced in the upper boundary layer due to entrainment mixing with dry air from above. Interestingly, q_v and θ profiles in D30 tend to evolve to the observed open-cell conditions. This is consistent with the cooling and moistening effects of evaporation of rain drops in the sub-cloud layer. The surface moisture fluxes also contribute to the lower-level high q_v in D30 but not as much as in D500 where the lower boundary layer is much less turbulent, as indicated by the contrast in vertical velocity variance in Fig. 4. For the same reason, simulations such as W30 and W150 that are initiated by the observed "wetter" sounding give much wetter and cooler profiles after precipitation occurs. Therefore, model results suggest that the observed marked differences in q_v and θ between overcast and open-cell regions can be explained by precipitation
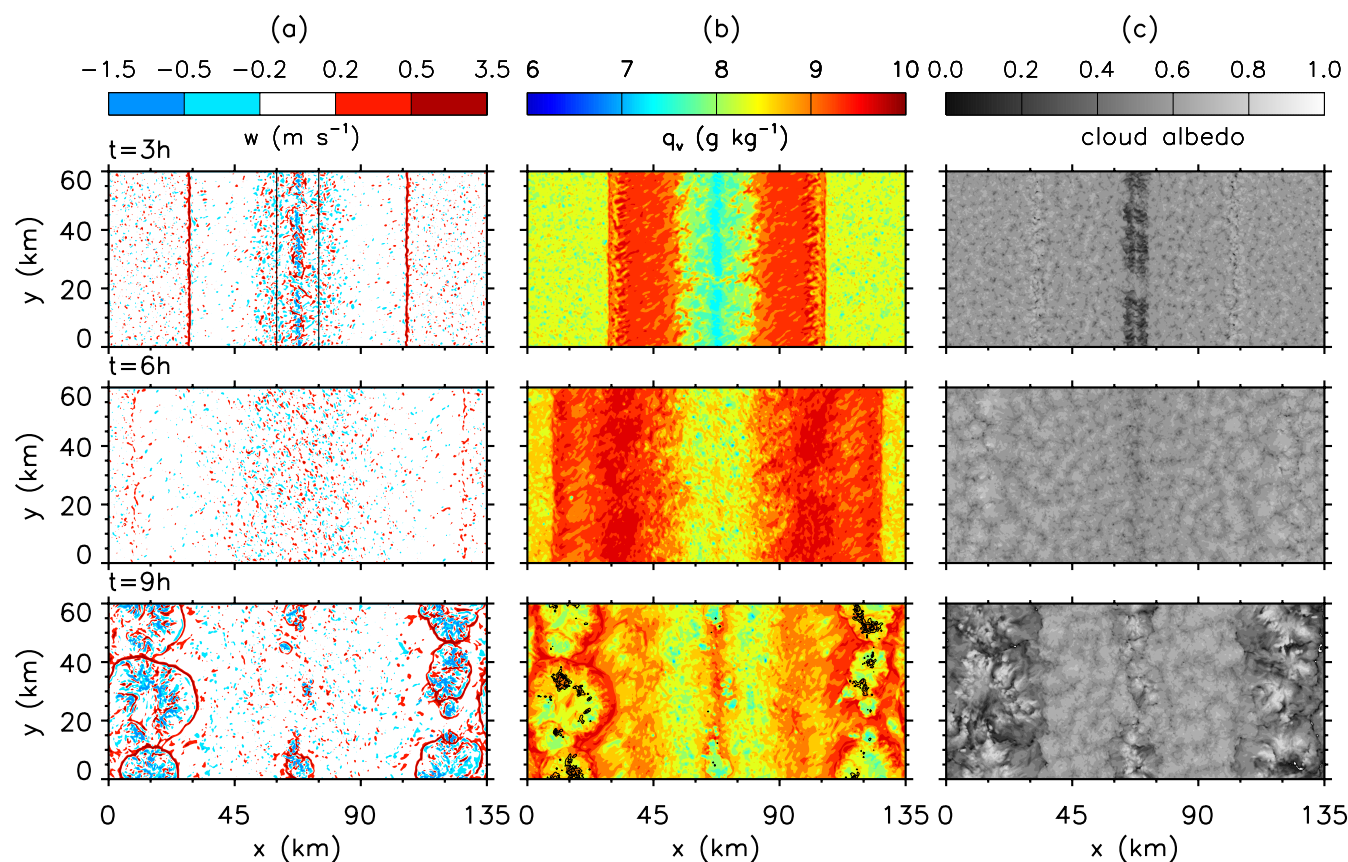
Fig. 11. Snapshots of **(a)** 200-m vertical velocity w, **(b)** 200-m water vapor mixing ratio q_v, and **(c)** cloud albedo at $t = 3$, 6 and 9 h (corresponding to each of the three rows) from experiment CTRL-QVT2; contours of rain rate (0.2, 5, and 20 mm day^{-1}) are superimposed on the q_v fields. Initial perturbations are applied to the 15-km strip marked in the upper-left panel.

and evaporation processes in the open-cell region. These processes are the direct cause of POC formation and the changes in q_v and θ. This, together with the monotonic decrease in aerosol concentration associated with coalescence scavenging and precipitation make POC-formation an un-buffered process.

5 Conclusions

Open cells, closed cells and pockets of open cells (POCs) are common cloud structures in the Southeast Pacific (SEP) stratocumulus region. Observations from the VAMOS Ocean-Cloud-Atmosphere-Land Study Regional Experiment (VOCALS-REx) support the hypothesis that drizzle is a necessary condition for the formation and maintenance of POCs within closed-cell stratocumulus. Nevertheless, what exactly initiates drizzle and POCs in the first place has been unclear. In this study, two sets of three-dimensional cloud-resolving simulations, based on observations from the C-130 Research Flight 6 during VOCALS-REx, are conducted (i) to examine diurnal variations of closed- and open-cell cloud properties

under different meteorological conditions; and (ii) to investigate the effectiveness of factors such as boundary-layer moisture and temperature perturbations, surface heat and moisture fluxes, large-scale vertical motion and solar heating at promoting drizzle and open cell formation.

Both open and closed cells simulated with observed initial conditions exhibit distinct diurnal variations in cloud fraction, liquid water path (LWP) and rain rate (if any) with a late-afternoon minimum. Solar heating due to short-wave absorption by cloud water and water vapor stabilizes the boundary layer and breaks up open-cell walls and the stratocumulus deck. If this breakup process is not accompanied by precipitation, closed cells can recover during the course of the following night. Within one diurnal cycle, for the open-cell cases considered, precipitation can deplete the initial aerosol to an extent that cloud formation is significantly suppressed. Even a CCN source strength of 0.72 mg^{-1} h^{-1} starting at 6 pm (local time) is sufficient to maintain clouds and prevent the boundary layer from collapsing the following day, suggesting that some local and/or remote aerosol source is necessary for POCs to be able to last for days.
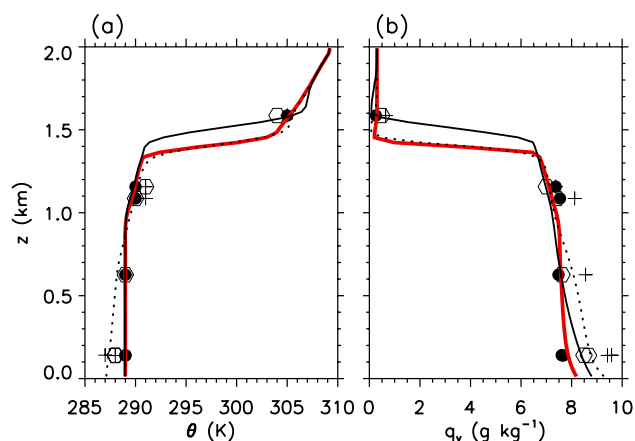
Fig. 12. Vertical profiles of **(a)** potential temperature θ and **(b)** water vapor mixing ratio q_v. Black circles, hexagons and plus signs represent RF06 leg-mean measurements for overcast regions, POCs and drizzling boundaries; Red lines are mean profiles during model spin-up time for both D30 and D500; Black solid lines (D500) and dotted lines (D30) are profiles averaged at night between $t = 3$ and 9 h.

Results show that drizzle and subsequent open cell formation over a broad region are more sensitive to the observed boundary-layer moisture and temperature perturbations ($+0.9$ g kg^{-1}; -1 K) than to a five-fold decrease in aerosol number concentration (150 vs. 30 mg^{-1}). When embedding the perturbations in closed cells, local drizzle and POC formation respond more rapidly to the aerosol reduction than to the moisture increase, but the latter gives stronger and more sustained drizzle. When a positive moisture perturbation and a negative temperature perturbation are combined, no drizzle is formed in the embedded area. This is because the local negative perturbation in temperature drives a mesoscale circulation that transports lower-level moisture out of the area; Drizzle is, however promoted in a remote area where lower-level horizontal transport of moisture is blocked and converges to enhance liquid water path. This represents a potential mechanism for POC formation in the Southeast Pacific stratocumulus region where the mesoscale circulation is triggered by strong precipitation and/or lower temperature in the nearby broad region of open cells.

Simulations of the approximate effects of an "upsidence wave" (with an amplitude of 0.01 m s^{-1}; Garreaud and Muñoz, 2004) exhibit significant increases in LWP (median value of 15 g m^{-2}), but this alone is not enough to initiate drizzle and POC formation in the moderately polluted environment. As seen in some other sensitivity experiments, even the organized smaller-scale, but much stronger updraft wave (on the order of 1 m s^{-1}) alone does not promote drizzle over the course of a few hours in the same environment. Thickening of the cloud ensures that these waves, when present in the SEP stratocumulus, create an environment more conducive

to drizzle and POC formation. Large increases in surface sensible heat flux and/or latent heat flux are also effective in triggering local drizzle and POC formation. Higher surface sensible heating enhances buoyancy of thermals and transports near-surface moisture to clouds more efficiently. This heating can also produce a temperature gradient and an associated local circulation that pumps moisture from neighboring areas. Additional moisture from the surface due to much larger surface latent heat fluxes is not as efficient at promoting drizzle immediately because it takes time for the moisture to reach clouds when it is not accompanied by stronger vertical transport. However, when both sensible and latent heat fluxes are enhanced, the impact is significant.

What exactly initiates drizzle in the open cells embedded in SEP closed cells? We hypothesize that strong precipitation in broad regions of open cells west of the SEP region, where aerosol concentrations are low and the sea surface temperature is warmer, may play a role in triggering POCs. At the scales simulated here (order 100 km) we have seen that certain perturbations can result in the formation of mesoscale flows that trigger open-cell formation in a remote region. It is conceivable that at larger scales, similar remote triggering mechanisms could occur. For example, lower-level outflow of moist air associated with strong precipitation could move eastward toward closed cells, converge with the prevailing easterly counter flow, or flow from a different source of precipitation, and significantly increase local cloud water. Moreover, the air in the outflow has lower CCN concentrations and is cooler and moves faster, promoting stronger surface sensible heat fluxes (with the assumption that ocean skin temperature does not vary significantly), all of which would increase the probability of drizzle in the convergence area. Once drizzle is initiated, open cell formation would become more widespread. Further work, including modeling at larger scales, and more rigorous model-observation comparisons, will be required to put this hypothesis on firmer footing.

References

Atkinson, B. W. and Zhang, J. W.: Mesoscale shallow convection in the atmosphere, Rev. Geophys., 34, 403–431, 1996.

Bretherton, C. S., Uttal, T., Fairall, C. W., Yuter, S. E., Weller, R., Baumgardner, D., Comstock, K. K., Wood, R., and Raga, G.: The EPIC 2001 stratocumulus study, B. Am. Meteorol. Soc., 85, 967–977, 2004.

Bretherton, C. S., Wood, R., George, R. C., Leon, D., Allen, G., and Zheng, X.: Southeast Pacific stratocumulus clouds, precipitation and boundary layer structure sampled along 20 S during VOCALS-REx, Atmos. Chem. Phys. Discuss., 10, 15921–15962, doi:10.5194/acpd-10-15921-2010, 2010.

Caldwell, P. and Bretherton, C. S.: Large eddy simulation of the diurnal cycle in Southeast Pacific stratocumulus, J. Atmos. Sci., 66, 432–449, 2009.

Clarke, A. D., Owens, S. R., and Zhou, J.: An ultrafine sea-salt flux from breaking waves: Implications for cloud condensation nuclei in the remote marine atmosphere, J. Geophys. Res., 111(D10), 6202, doi:10.1029/2005JD006565, 2006.

Comstock, K. K., Bretherton, C. S., and Yuter, S. E.: Mesoscale variability and drizzle in southeast Pacific stratocumulus, J. Atmos. Sci., 62, 3792–3807, 2005.

Dudhia, J.: Numerical study of convection observed during the winter monsoon experiment using a mesoscale two-dimensional model, J. Atmos. Sci., 46, 3077–3107, 1989.

Feingold, G., Walko, R. L., Stevens, B., and Cotton, W. R.: Simulations of marine stratocumulus using a new microphysical parameterization scheme, Atmos. Res., 47–48, 505–528, 1998.

Feingold, G.: Modeling of the first indirect effect: Analysis of measurement requirement, Geophys. Res. Lett., 30(19), 1997, doi:10.1029/2003GL017967, 2003.

Garay, M. J., Davies, R., Averill, C., and Westphal, J. A.: Actinoform clouds: Overlooked examples of cloud self-organization at the mesoscale. B. Am. Meteorol. Soc., 85, 1585–1594, 2004.

Garreaud, R. D. and Muñoz, R.: The diurnal cycle of circulation and cloudiness over the subtropical southeast Pacific: A modeling study, J. Climate, 17, 1699–1710, 2004.

Kubar, T., Hartmann, D. L., and Wood, R.: Understanding the importance of microphysics and macrophysics for warm rain in marine low clouds. Part I: Satellite observations, J. Atmos. Sci., 66, 2953–2972, 2009.

Mlawer, E. J., Taubman, S. J., Brown, P. D., Iacono, M. J., and Clough, S. A.: Radiative transfer for inhomogeneous atmospheres: RRTM, a validated correlated-k model for the longwave, J. Geophys. Res., 102(D14), 16663–16682, 1997.

Nicholls, S.: The dynamics of stratocumulus: aircraft observations and comparisons with a mixed layer model, Q. J. Roy. Meteorol. Soc., 110, 783–820, 1984.

Pawlowska, H. and Brenguier, J.-L.: An observational study of drizzle formation in stratocumulus clouds for general circulation model (GCM) parameterizations, J. Geophys. Res., 108(D15), 8630, doi:10.1029/2002JD002679, 2003.

Petters, M. D., Snider, J. R., Stevens, B., Vali, G., Faloona, I., and Russell, L. M.: Accumulation mode aerosol, pockets of open cells, and particle nucleation in the remote subtropical Pacific marine boundary layer, Geophys. Res. Lett., D02206. doi:10.1029/2004JD005694, 2006.

Rahn, D. A. and Garreaud, R. D.: Marine boundary layer over the subtropical southeast Pacific during VOCALS-REx. Part 1: Mean structure and diurnal cycle, Atmos. Chem. Phys., 10, 4491–4506, doi:10.5194/acp-10-4491-2010, 2010.

Savic-Jovcic, V. and Stevens, B.: The structure and mesoscale organization of precipitating stratocumulus, J. Atmos. Sci., 65, 1587–1605, 2008.

Sharon, T. M., Albrecht, B. A., Jonsson, H. H., Minnis, P., Khaiyer, M. M., van Reken, T. M., Seinfeld, J., and Flagan, R.: Aerosol and cloud microphysical characteristics of rifts and gradients in maritime stratocumulus clouds, J. Atmos. Sci., 63, 983–997, 2006.

Sorooshian, A., Feingold, G., Lebsock, M., Jiang, H., and Stephens, G.: On the precipitation susceptibility of clouds to aerosol perturbations, Geophys. Res. Lett., 36, L13803, doi:10.1029/2009GL038 993, 2009.

Stevens, B., Cotton, W. R., Feingold, G., and Moeng, C.-H.: Large-eddy simulations of strongly precipitating, shallow, stratocumulus-toped boundary layers, J. Atmos. Sci., 55, 3616–3638, 1998.

Stevens, B. and Feingold, G.: Untangling aerosol effects on clouds and precipitation in a buffered system, Nature, 461, 607–613, 2009.

Stevens, B., Moeng, C.-H., Ackerman, A. S., and coauthors: Evaluation of large-eddy simulations via observations of nocturnal marine stratocumulus, Mon. Weather Rev., 133, 1443–1462, 2005a.

Stevens, B., Vali, G., Comstock, K. K., vanZanten, M. C., Austin, P. H., Bretherton, C. S., and Lenschow, D. H.: Pockets of open cells (POCs) and drizzle in marine stratocumulus, B. Am. Meteorol. Soc., 86, 51–57, 2005b.

vanZanten, M. C., Stevens, B., Vali, G., and Lenschow, D. H.: Observations of drizzle in nocturnal marine stratocumulus, J. Atmos. Sci., 62, 88–106, 2005.

Wang, H. and Feingold, G.: Modeling mesoscale cellular structures and drizzle in marine stratocumulus. Part I: Impact of drizzle on the formation and evolution of open cells, J. Atmos. Sci., 66, 3237–3256, 2009a.

Wang, H. and Feingold, G.: Modeling mesoscale cellular structures and drizzle in marine stratocumulus. Part II: The microphysics and dynamics of the boundary region between open and closed cells, J. Atmos. Sci., 66, 3257–3275, 2009b.

Wang, H. and McFarquhar, G. M.: Large-eddy simulations of the diurnal cycle of shallow convection and cloudiness over the tropical Indian Ocean, Q. J. Roy. Meteorol. Soc., 134, 643–661, 2008.

Wang, H., Skamarock, W. C., and Feingold, G.: Evaluation of scalar advection schemes in the Advanced Research WRF model using large-eddy simulations of aerosol-cloud interactions, Mon. Weather Rev., 137, 2547–2558, 2009.

Wood, R. and Hartmann, D. L.: Spatial variability of liquid water path in marine low cloud: The importance of mesoscale cellular convection, J. Climate, 19, 1748–1764, 2006.

Wood, R., Comstock, K. K., Bretherton, C. S., Cornish, C., Tomlinson, J., Collins, D. R., and Fairall, C. W.: Open cellular structure in marine stratocumulus sheets, J. Geophys. Res., 113, D12207, doi:10.1029/2007JD009371, 2008.

Wood, R., Bretherton, C. S., Leon, D., Clarke, A. D., Zuidema, P., Allen, G., and Coe, H.: An aircraft case study of the spatial transition from closed to open mesoscale cellular convection, Atmos. Chem. Phys. Discuss., submitted, 2010.

Wood, R., Bretherton, C. S., Mechoso, C. R., and coauthors: The VAMOS Ocean-Cloud-Atmosphere-Land Study Regional Ex-

periment (VOCALS-REx): Goals, platforms and field operations, Atmos. Chem. Phys. Discuss., to be submitted, 2010.

Wood, R., Kubar, T., and Hartmann, D. L.: Understanding the importance of microphysics and macrophysics for warm rain in marine low clouds. Part II: Heuristic models of rain formation, J. Atmos. Sci., 66, 2973–2990, 2009.

Xue, H., Feingold, G., and Stevens, B.: Aerosol effects on clouds, precipitation, and the organization of shallow cumulus convection, J. Atmos. Sci., 65, 392–406, 2008.